Heating and cooling of the thermosphere by internal gravity waves

Erdal Yiğit[1,2,3] and Alexander S. Medvedev[2]

Received 3 April 2009; revised 10 June 2009; accepted 17 June 2009; published 21 July 2009.

[1] For the first time, estimates of heating and cooling in the upper thermosphere due to dissipating and breaking gravity waves (GWs) of tropospheric origin have been obtained with a comprehensive general circulation model (GCM). A GW parameterization specifically designed for thermospheric heights has been implemented in the CMAT2 GCM covering altitudes from the tropopause to the F_2 region, and simulations for the June solstice have been performed. They reveal that the net thermal effect of GWs above the turbopause is cooling. The largest (up to -170 K d^{-1} in a zonally and temporally averaged sense) cooling takes place in the high latitudes of both hemispheres near 210 km. The instantaneous values of heating and cooling rates are highly variable, and reach up to 500 and -3000 K d^{-1} in the F_2 region, respectively. Inclusion of the GW thermal effects reduces the simulated model temperatures by up to 200 K over the summer pole and by 100 to 170 K at other latitudes near 210 km. **Citation:** Yiğit, E., and A. S. Medvedev (2009), Heating and cooling of the thermosphere by internal gravity waves, *Geophys. Res. Lett.*, *36*, L14807, doi:10.1029/2009GL038507.

1. Introduction

[2] Dissipating and/or breaking gravity waves (GWs) produce heating of the mean flow [*Gavrilov*, 1990; *Becker and Schmitz*, 2002; *Medvedev and Klaassen*, 2003], and induce a downward sensible heat flux [*Walterscheid*, 1981; *Medvedev and Klaassen*, 2003]. The former effect is the result of irreversible conversion of mechanical wave energy into heat. The latter arises due to altering the phase relationship between wave fluctuations of temperature and vertical velocity by the diffusivity associated with GW dissipation/breaking. Thermal effects of internal GWs generated in the troposphere have been studied in the mesosphere-lower thermosphere (MLT) using comprehensive general circulation models (GCMs) [*Medvedev and Klaassen*, 2003; *Becker*, 2004]. It was found that during solstices, GWs can produce monthly mean cooling rates up to several K d^{-1} in the lower thermosphere and a somewhat weaker heating below. These values are comparable with radiative heating/cooling rates, and should not be neglected in the MLT energy budget.

[3] Although a growing number of observations indicates that the thermosphere-ionosphere (TI) system is continuously perturbed by GWs propagating from below [*Forbes*, 2007], systematic estimates have not been attempted at these heights, to the best of our knowledge. Among possible reasons for this deficiency are that thermosphere GCMs either do not couple the troposphere with the upper atmosphere, or they lack appropriate GW parameterizations that can realistically account for wave dissipation above the turbopause. Recently, we have developed a suitable spectral GW scheme [*Yiğit et al.*, 2008] and implemented it in the Coupled Middle Atmosphere-Thermosphere-2 (CMAT2) GCM [*Yiğit et al.*, 2009]. It has been shown that dynamical effects of GWs propagating from below are not only non-negligible in the TI, but are comparable with those of ion friction, at least below 180–200 km. In this paper, we turn our attention to thermal effects of dissipating internal GWs of lower atmospheric origin, estimate them, and assess their role in the TI. This is done with numerical experiments employing the CMAT2 GCM and the spectral GW parameterization.

2. Model Description

[4] We use the version of CMAT2 described in detail by *Yiğit et al.* [2009]. The model domain extends from the lower stratosphere (100 hPa, or $\sim$15 km) to the upper thermosphere (typically 1.43×10^{-8} hPa, or $\sim$250–600 km) with 63 vertical levels (1/3 scale height discretization), and a $2^\circ \times 18^\circ$ latitude-longitude resolution. The model parameterizations account for the absorption of solar radiation by ozone in the Chappuis, Huggins, and Hartley bands; by O_2 in the Schumann-Runge bands, and for heating due to the exothermic neutral chemistry. Thermospheric heating, photodissociation, and photoionization are calculated for the absorption of solar X-rays, EUV, and UV radiation between 1.8–184 nm. Radiative cooling parameterizations include the 5.3 μm NO, 63 μm fine structure atomic oxygen, local thermodynamic equilibrium (LTE) and non-LTE 15.6 μm CO_2, and 9.6 μm O_3 radiative emissions. The model incorporates appropriate representations of electric fields, auroral particle precipitation at high latitudes, Joule heating, and ion drag. The morphology of the ionospheric electron density is taken from the Parameterized Ionospheric Model (PIM) [*Daniell et al.*, 1995]. In the numerical experiments to be presented, we use prescribed climatological distributions of chemical species and of the Earth's magnetic field. CMAT2 lacks a troposphere and, as was described in the work by *Yiğit et al.* [2009], is forced at the lower boundary by the NCEP reanalysis data and tidal oscillations from the Global Scale Wave Model-02 [*Hagan and Forbes*, 2003].

3. Results

[5] The utilized spectral GW scheme is essentially the same as was described in detail by *Yiğit et al.* [2008, 2009].

[1]Department of Atmospheric, Oceanic and Space Sciences, University of Michigan, Ann Arbor, Michigan, USA.
[2]Max Planck Institute for Solar System Research, Katlenburg-Lindau, Germany.
[3]Atmospheric Physics Laboratory, Department of Physics and Astronomy, University College London, London, UK.

0094-8276/09/2009GL038507

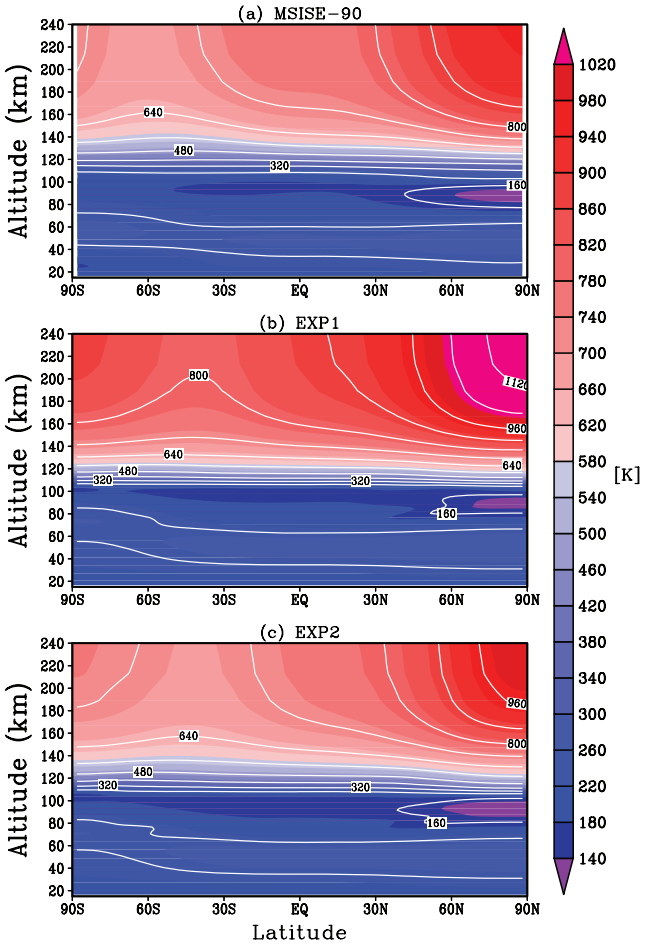

Figure 1. Zonal mean temperature averaged over the period between 16 June and 6 July: (a) from the empirical MSISE-90 model; (b) from EXP1 without GW heating/cooling; (c) from EXP2 including the GW heating/cooling. White contour lines mark temperature in 80 K intervals.

The amplitudes of wave momentum fluxes for harmonics with the same horizontal wavelength (λ_h = 300 km) and different phase velocities, c_i, were kept constant at all times and geographical locations throughout the simulations. The morphology of this spectrum [*Yiğit et al.*, 2009, Figure 1] is in a very good agreement with the balloon measurements of *Hertzog et al.* [2008, Figure 6]. Additionally, we assumed that horizontal phase velocities of GW harmonics were aligned along the direction of the local wind at the source level, both up- and down the wind. As was absolutely correctly noticed by S. Vadas, this source setup excluded many of high-frequency and short-scale harmonics generated by convection. Vertical propagation of individual harmonics with the horizontal phase speed c_i and the resulting momentum deposition rate ("wave drag") a_i were calculated for all grid points. The total thermal effect of a harmonic consists of the heating due to wave dissipation, E_i, and the differential heating/cooling, Q_i, associated with the divergence of wave-induced heat flux, [*Yiğit et al.*, 2008, equation (6)]:

$$E_i = c_p^{-1} a_i (c_i - \bar{u}), \qquad Q_i = \frac{H}{2\rho R}\frac{\partial}{\partial z}[\rho a_i (c_i - \bar{u})], \qquad (1)$$

where c_p is the specific heat at constant pressure, H is the density scale height, R is the gas constant, and ρ is the background mass density. Unlike in the work by *Yiğit et al.* [2009], contributions of all subgrid-scale harmonics were not omitted here, but served as a forcing in the thermodynamic equation for resolved fields in CMAT2.

[6] We compare two model experiments: a) without (EXP1) and b) with the included GW heating/cooling (EXP2). In both cases, CMAT2 was run from the equinox (21 March) till 6 July, and 4-hour outputs around the solstice were analyzed. The geomagnetic and solar activity were kept at constant low values ($F_{10.7}$ = 80 × 10^{-22} W m^{-2} Hz^{-1}; K_p = 2^+) at all times to eliminate possible uncertainties associated with their variations. The mean effects of GW-induced heating rates on the simulated temperature are illustrated in Figure 1. For that, the model fields were averaged over the last 21 days of the simulations, that is between 16 June and 6 July. For comparison, the temperature from the empirical MSISE-90 model was processed in a similar manner, and is plotted in Figure 1a. It is seen that the coldest (<140 K) temperature in the entire model domain is found in the summer mesopause, while the hottest (>900 K) is in the high-latitude summer upper thermosphere. Figure 1b shows the zonal mean zonal temperature from the run without GW heating/cooling (EXP1). Although CMAT2 captures the mean temperature structure reasonably well compared to MSISE-90, especially below the turbopause (<105 km), the simulated upper thermospheric temperatures are noticeably higher. There are many possible reasons for this overestimate, which are related to uncertainties in radiation parameterizations, input data, and the use of climatological distributions of radiatively active species. In particular, our own numerical experiments demonstrated a high sensitivity to variations of the atomic oxygen and of the adopted value of the collisional quenching rate [*Castle et al.*, 2006]. The temperature simulated in the run including the GW heating/cooling (EXP2, Figure 1c) reveals much better agreement with MSISE-90. It is seen that the overall thermal effect of GWs above the tropopause is cooling. The warm temperature bias is reduced in EXP2 by more than 200 K over the summer pole near the model top and by 100 to 170 K at other latitudes in the thermosphere.

[7] Detailed illustrations of the GW heating and cooling rates and their comparisons with other diabatic effects are given in Figure 2. The irreversible heating E_i (Figure 2a) is large in the high latitudes of both hemispheres and peaks at 90 to 100 K d^{-1} near 200–210 km. The secondary peak of up to 10 K d^{-1} is located in the tropics below 130–140 km. Note that the areas of enhanced GW heating do not precisely coincide with those of wave drag. The latter is distributed relatively uniformly in latitude [*Yiğit et al.*, 2009, Figure 3b] with maxima in midlatitudes. However, due to strong filtering below, this drag in the high latitudes is created by "surviving" harmonics with high phase speeds traveling against the mean wind, i.e. by those with high $|c_i - \bar{u}|$. This explains large magnitudes of $(c_i - \bar{u})a_i$ at high-latitudes, and, therefore, strong GW heating and cooling. For example, unlike with E_i, the drag has two thermospheric maxima in each hemisphere: in the middle- and high-latitudes as well as a weaker maximum over the equator below 130 km [*Yiğit et al.*, 2009, Figure 3b]. The role of the GW-induced heating

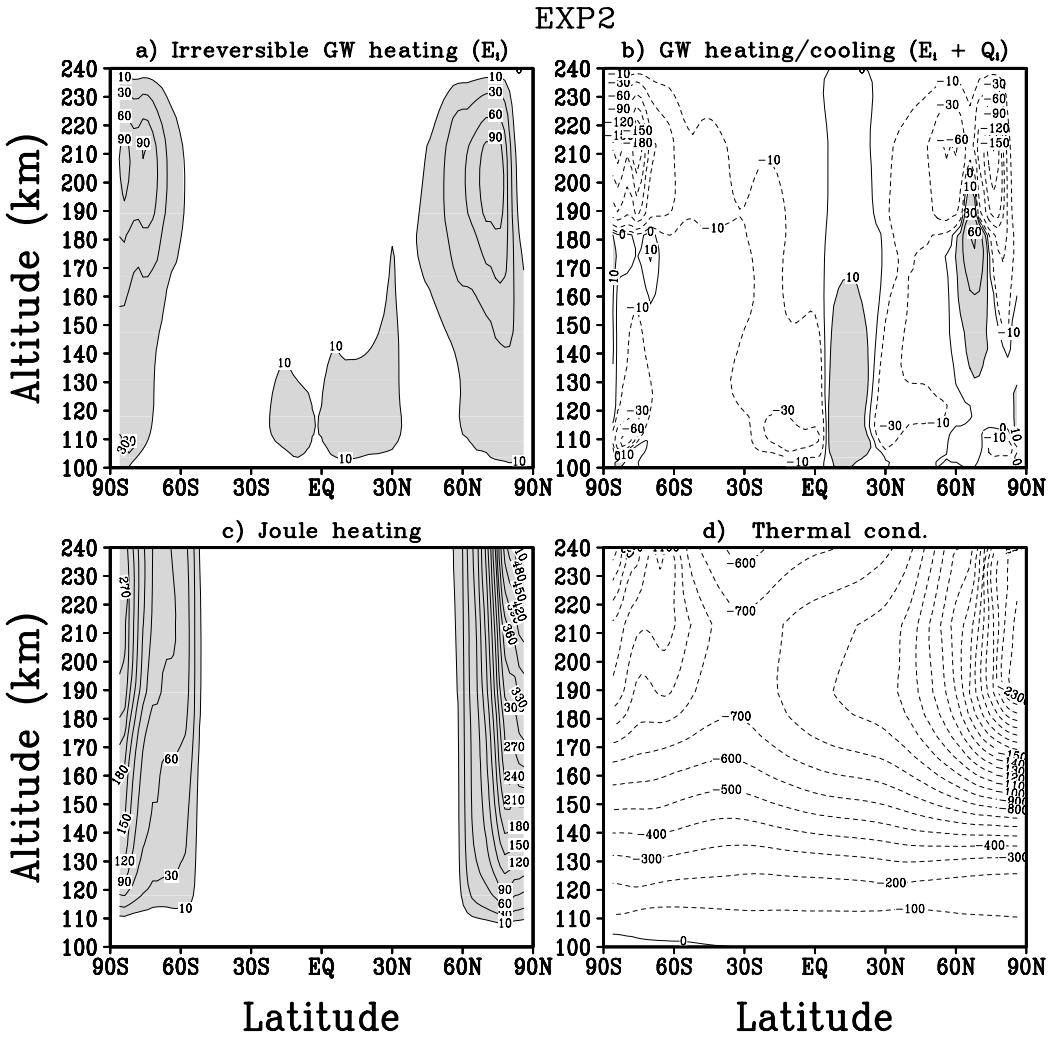

Figure 2. 21-day averaged zonal mean heating/cooling rates simulated with CMAT2 (in K d^{-1}): (a) irreversible GW heating (E); (b) total GW heating/cooling ($E + Q$); (c) Joule heating; (b) cooling due to molecular thermal conduction. Shaded are the positive values.

is clearly seen when compared with the Joule heating. The latter occurs due to collisions between charged and neutral particles, and is an important diabatic heating mechanism in the TI. The corresponding heating rates (Figure 2c) are up to 250 and 400 K d^{-1} in the southern and northern hemispheres (SH and NH), respectively. Stronger heating in the NH is largely due to higher ionization rates in the summer hemisphere. Hence, in the high latitudes, the contribution of GWs is between 20 and 40% of that by the Joule heating.

[8] However, the net effect of GWs is dominated by cooling, especially in the upper thermosphere. As can be seen from Figure 2b, the maxima of ~ -180 and ~ -150 K d^{-1} are formed at around 210 km in the high latitudes of the SH and NH, respectively. There is also an area of marked GW cooling of up to -60 K d^{-1} in the midlatitudes of the NH. Areas of the net GW heating (up to 60 K d^{-1} in the NH) lie just below. It follows from Figures 2a and 2b that they are created by the differential heating/cooling Q, which tends to redistribute the mean potential temperature vertically through GW-induced downward heat fluxes. In our simulations, the differential cooling can reach up to -250 and -270 K d^{-1} at 200 km in the high latitudes. The main cooling mechanism in the upper thermosphere is the molecular thermal conduction. The corresponding rates (up to -1100 and -2300 K d^{-1} in the SH and NH, respectively) are plotted in Figure 2d. It is seen that GW cooling can increase up to 10 and 20% of that by molecular heat conduction.

[9] Having considered averaged thermal effects of GWs, we now focus on their temporal and spatial variability. Our simulations show that instantaneous values of the GW-related heating and cooling rates can significantly exceed the mean quantities discussed above. To illustrate the extent of variations, we present few typical distributions from the CMAT2 output on 22 June. The height-universal time (UT) cross-sections of the temperature and total GW heating rates Σ_i ($E_i + Q_i$) are plotted in Figures 3a and 3b for two fixed geographical locations (75°S, 140°W) and (75°N, 140°W). These points have been chosen because enhanced GW activity occurs in the high latitudes. A strong dipole pattern of heating below $\sim$190 km and cooling above is seen between the local midnight and noon at 75°S. The heating rates reach up to 500 K d^{-1} at 170–180 km and cooling exceeds -1000 K d^{-1} near $\sim$210 km. A reversed but significantly weaker heating/cooling structure takes place during the other half of the day. This day-night asymmetry

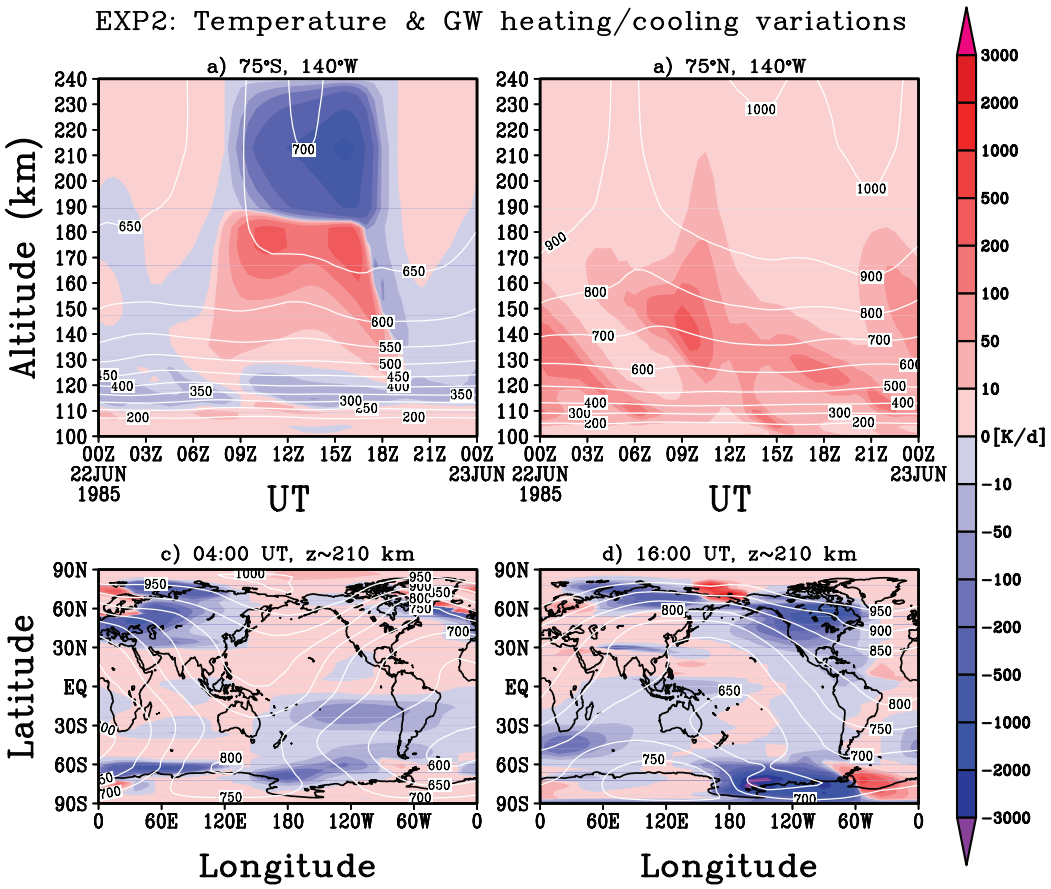

Figure 3. The total GW heating/cooling rates (color-shaded) and temperature (white contour lines) simulated with CMAT2 on 22 June: height-Universal time (UT) variations at (a) 75°S, 140°W and (b) 75°N, 140°W; geographical distributions at (c) 0400 UT and (d) 1600 UT.

contributes to the daily and zonally averaged rates shown in Figure 2d. The variations of heating rates are closely related to the modulation of the GW drag by the diurnal tide, as was discussed in section 9 of the work by *Yiğit et al.* [2009]. Two strong peaks of westerly momentum deposition at ~10 UT and 16 UT (not shown here) take place at 200–210 km, just above the altitude that divides the regions of GW heating and cooling. In the given longitude point of the high-latitude NH, the total effect of GW heating is modulated by both diurnal and semi-diurnal tides, with maxima of about 500 K d^{-1} at 140 km.

[10] Snapshots of the GW-induced heating/cooling rates at 210 km in Figures 3c and 3d illustrate an extent of the spatial and temporal variability of the latter. The two distributions, which are 12 hours apart, demonstrate that most of the variations are associated with the sun-synchronous diurnal tides, especially in the mid- and high latitudes in both hemispheres. Locally, the thermal effects of GWs can significantly exceed the average values. For example, an enhanced cooling of more than 3000 K d^{-1} at 150°W in the SH appears particularly striking.

4. Summary and Conclusions

[11] Heating and cooling of the thermosphere by breaking and/or dissipating small-scale internal gravity waves have been studied for the first time using a comprehensive GCM extending from the tropopause to the F_2 region. A spectral nonlinear GW parameterization suitable for these heights [*Yiğit et al.*, 2008] has been implemented in the CMAT2 GCM and estimates of GW-induced heating/cooling rates for the June solstice have been obtained under low geomagnetic and solar activity conditions.

[12] The irreversible heating due to wave energy dissipation is strong (up to 100 K d^{-1} in zonally and temporally averaged sense) in the high latitudes of both hemispheres, which constitutes between 20 and 40% of that by the Joule heating. However, the net thermal effect of GWs above the turbopause is dominated by cooling associated with the divergence of the induced downward heat flux. The maxima of −150 to −180 K d^{-1} occur also in the high latitudes around 210 km. When the total GW heating and cooling are taken into account in the GCM, the simulated thermospheric temperatures become colder: up to 200 K over the summer pole, and up to 100 to 170 K at other latitudes near 210 km.

[13] Instantaneous values of GW heating and cooling rates are highly variable, and can significantly exceed the averaged quantities. In our simulations they can easily reach up to 500 and −1100 K d^{-1} and even more than −3000 K d^{-1} locally in the F_2 region. Most of variations and largest heating/cooling rates take place in the high latitudes of both hemispheres, and are strongly modulated by solar tides.

[14] It must be noted that GW effects in the upper thermosphere, both dynamical [*Yiğit et al.*, 2009] and

thermal, are highly sensitive to the amount of momentum prescribed to high phase speed GW harmonics in the source spectrum. In our simulations, we used very moderate constant values at the source level that are close to the mean observed quantities [*Hertzog et al.*, 2008] and are typically employed in GCMs. However, convection can generate fast GWs with amplitudes much higher than those used here [*Song and Chun*, 2005]. Therefore, our results can be viewed as very modest estimates, perhaps even underestimates, of GW-induced heating/cooling rates in the thermosphere. Measurements of GW fluxes in the thermosphere and application of more sophisticated parameterizations of wave sources in the lower atmosphere can help to quantify GW thermal effects further.

[15] The overall conclusion of this work is that heating and cooling by dissipating GWs propagating from below significantly contribute to the thermal balance of the thermosphere above the turbopause. They should not be neglected in the thermosphere GCMs.

[16] **Acknowledgments.** This work was partially supported by the German Science Foundation (DFG), project HA3261/4,5, and by AFOSR grant FA9550-07-1-0434.

References

Becker, E. (2004), Direct heating rates associated with gravity wave saturation, *J. Atmos. Sol. Terr. Phys.*, *66*, 683–696.

Becker, E., and G. Schmitz (2002), Energy deposition and turbulent dissipation owing to gravity waves in the mesosphere, *J. Atmos. Sci.*, *59*, 54–68.

Castle, K. J., K. M. Kleissas, J. M. Rhinehart, E. S. Hwang, and J. A. Dodd (2006), Vibrational relaxation of $CO_2(\nu_2)$ by atomic oxygen, *J. Geophys. Res.*, *111*, A09303, doi:10.1029/2006JA011736.

Daniell, R. E., L. D. Brown, D. N. Anderson, M. W. Fox, P. H. Doherty, D. T. Decker, J. J. Sojka, and R. W. Schunk (1995), PIM: A global ionospheric parameterization based on first principles models, *Radio Sci.*, *30*, 1499–1510.

Forbes, J. M. (2007), Dynamics of the upper mesosphere and thermosphere, *J. Meteorol. Soc. Jpn.*, *85*, 193–213.

Gavrilov, N. M. (1990), Parameterization of accelerations and heat flux divergences produced by internal gravity waves in the middle atmosphere, *J. Atmos. Terr. Phys.*, *52*, 707–713.

Hagan, M. E., and J. M. Forbes (2003), Migrating and nonmigrating semidiurnal tides in the middle and upper atmosphere excited by tropospheric latent heat release, *J. Geophys. Res.*, *108*(A2), 1062, doi:10.1029/2002JA009466.

Hertzog, A., G. Boccara, R. A. Vincent, F. Vial, and P. Cocqurez (2008), Estimation of gravity wave momentum flux and phase speeds from quasi-Lagrangian stratospheric balloon flights. Part II: Results from Vorcore campaign in Antarctica, *J. Atmos. Sci.*, *65*, 3056–3070.

Medvedev, A. S., and G. P. Klaassen (2003), Thermal effects of saturating gravity waves in the atmosphere, *J. Geophys. Res.*, *108*(D2), 4040, doi:10.1029/2002JD002504.

Song, I.-S., and H.-Y. Chun (2005), Momentum flux spectrum of convectively forced internal gravity waves and its application to gravity wave drag parameterization. Part I: Theory, *J. Atmos. Sci.*, *62*, 107–124.

Walterscheid, R. L. (1981), Dynamical cooling induced by dissipating internal gravity waves, *Geophys. Res. Lett.*, *8*, 1235–1238.

Yiğit, E., A. D. Aylward, and A. S. Medvedev (2008), Parameterization of the effects of vertically propagating gravity waves for thermosphere general circulation models: Sensitivity study, *J. Geophys. Res.*, *113*, D19106, doi:10.1029/2008JD010135.

Yiğit, E., A. S. Medvedev, A. D. Aylward, P. Hartogh, and M. J. Harris (2009), Modeling the effects of gravity wave momentum deposition on the general circulation above the turbopause, *J. Geophys. Res.*, *114*, D07101, doi:10.1029/2008JD011132.

A. S. Medvedev, Max Planck Institute for Solar System Research, Max-Planck-Str. 2, D-37191 Katlenburg-Lindau, Germany. (medvedev@mps.mpg.de)

E. Yiğit, Department of Atmosphere, Oceanic and Space Sciences, University of Michigan, 1429 Space Research Building, 2455 Hayward Street, Ann Arbor, MI 48109-2143, USA. (erdal@umich.edu)